Published online 16 August 2013 *Nucleic Acids Research, 2013, Vol. 41, No. 20* ***9557–9569***
doi:10.1093/nar/gkt705

Identification and characterization of a hitherto unknown nucleotide-binding domain and an intricate interdomain regulation in HflX-a ribosome binding GTPase

Nikhil Jain, Neha Vithani, Abu Rafay and Balaji Prakash*

Department of Biological Sciences and Bioengineering, Indian Institute of Technology Kanpur, Kanpur 208106, India

Received March 8, 2013; Revised July 17, 2013; Accepted July 18, 2013

ABSTRACT

A role for HflX in 50S-biogenesis was suggested based on its similarity to other GTPases involved in this process. It possesses a G-domain, flanked by uncharacterized N- and C-terminal domains. Intriguingly, *Escherichia coli* HflX was shown to hydrolyze both GTP and adenosine triphosphate (ATP), and it was unclear whether G-domain alone would explain ATP hydrolysis too. Here, based on structural bioinformatics analysis, we suspected the possible existence of an additional nucleotide-binding domain (ND1) at the N-terminus. Biochemical studies affirm that this domain is capable of hydrolyzing ATP and GTP. Surprisingly, not only ND1 but also the G-domain (ND2) can hydrolyze GTP and ATP too. Further; we recognize that ND1 and ND2 influence each other's hydrolysis activities via two salt bridges, i.e. E29-R257 and Q28-N207. It appears that the salt bridges are important in clamping the two NTPase domains together; disrupting these unfastens ND1 and ND2 and invokes domain movements. Kinetic studies suggest an important but complex regulation of the hydrolysis activities of ND1 and ND2. Overall, we identify, two separate nucleotide-binding domains possessing both ATP and GTP hydrolysis activities, coupled with an intricate inter-domain regulation for *Escherichia coli* HflX.

INTRODUCTION

GTPases play key roles in regulating several biological processes, both in prokaryotes and eukaryotes. Based on rigorous analysis of sequences, Leipe *et al.* (1) classified GTPases into several classes and families; HflX was classified under the Obg-HflX super-family, which comprises a group of ancient GTPases of the translation factor-related GTPase class. Phylogenetic analysis of HflX homologues revealed that it is largely conserved in all three kingdoms of life, excepting for some species like *Mycoplasma*, the epsilon subdivision of Proteobacteria, *Spirochaetes*, the archaeon *Methanobacterium* and fungi (1).

A wide taxonomic distribution suggests a central role for HflX. It shares several similarities to bacterial GTPases that interact with the ribosomal subunits; some of which are known to play key roles in ribosome biogenesis (2). Among these, RbgA, YsxC, ObgE and YphC are implicated in the biogenesis of 50S (3–7), whereas Era, RsgA and YqeH were shown to be involved in 30S biogenesis (8–10). Most of these multi-domain proteins possess a single nucleotide-binding domain and bind ribosomal subunits in a GTP-dependent manner (11).The only exception to these is EngA that has two contiguous G domains (GD1 and GD2) (6). Altering the nucleotides bound at GD1 and GD2 invokes large domain movements that appear to enable EngA to exist in two distinct ribosome bound states, i.e. bound to 50S alone or that bound to 50S, 30S and 70S subunits (12). HflX, like several ribosome-binding GTPases, was shown to interact with 50S alone, but this binding is noted in all nucleotide bound states (13,14). Interestingly, recent reports suggest that HflX interacts not only with 50S but also with 30S and 70S (15). This prompted us to investigate the interplay, if any, between the various domains present in HflX.

Combining structural bioinformatics and biochemical studies, here we attempt to understand structure-function relationship in HflX, by characterizing its various domains and examining their possible biochemical roles. *Escherichia coli* HflX (EcHflX) comprises three

*To whom correspondence should be addressed. Tel: +91 512 2594024; Fax: +91 512 2594010; Email: bprakash@iitk.ac.in
Present address:
Nikhil Jain, Department of Microbiology and Molecular Genetics, Michigan State University, East-Lansing, MI 48823 USA.

© The Author(s) 2013. Published by Oxford University Press.
This is an Open Access article distributed under the terms of the Creative Commons Attribution Non-Commercial License (http://creativecommons.org/licenses/by-nc/3.0/), which permits non-commercial re-use, distribution, and reproduction in any medium, provided the original work is properly cited. For commercial re-use, please contact journals.permissions@oup.com

domains—a GTPase domain sandwiched between uncharacterized N- and C-terminal domains, termed NTD and CTD, respectively. NTD is conserved among HflX homologues, wherease CTD, being absent in a few species like *Sulfolobus solfataricus,* is not well conserved. The G-domain in HlfX conserves the G1-G4 motifs, known to be important for GTP binding and hydrolysis (16). G1, also called the P-loop, contains an essential lysine residue that interacts with the β and γ phosphates of GTP (Supplementary Figure S1), and its mutation is known to disrupt nucleotide binding (17). G2 (switch-I) and G3 (switch II) sense the GTP versus GDP bound states and acquire specific conformations; an aspartate in the G4 (NKXD) determines the specificity for Guanine nucleotide (18).

Given that the G4 motif in HflX is NKID, it is surprising that EcHflX was reported to bind and hydrolyze not only GTP (which is anticipated) but also adenosine triphosphate (ATP) (13,19). Among the other prokaryotic ribosome binding GTPases, YchF similarly conserves the G4 motif (NVNE), but it binds and hydrolyzes ATP better than GTP (20). We anticipated that the ^{317}NKID^{320} motif in EcHflX would preferentially recognize guanine nucleotides at the G-domain; we also found significant ATP hydrolysis activity (13). In contrast, Shields *et al*. (21) compared the affinities for ATP and GTP and proposed that HflX prefers GTP over ATP. This inference was based on kinetic studies. Following the binding of fluorescently labeled mant-ATP, a significant FRET signal between the mant group and a trp residue, present near the active site, could not be detected by Shields and co-workers: The work presented here was initiated to further clarify ATP versus GTP binding in HflX.

We set out to investigate ATP hydrolysis by HflX. To begin with, we wondered if region(s) neighboring the G-domain could be responsible for ATP binding and hydrolysis. Here, we report a hitherto unknown nucleotide-binding domain (called ND1) in HflX and demonstrate that both ND1 and ND2 (i.e. the G-domain) are domains that hydrolyze GTP as well as ATP, albeit with different efficiencies. Besides this, we also demonstrate the significance of two important salt bridges at the inter-domain interface, in the regulation of GTP/ATP hydrolysis activities of ND1 and ND2 (22). These salt bridges clamp the two domains together, and their disruption induces domain movements, as inferred from the exposure of an otherwise buried cysteine at the interface of ND1 and ND2. Domain deletion studies also decipher important but complex regulation imposed by one domain on the other domain's activity. Understanding this inter-domain regulation and how it influences GTPase and ATPase activities might be vital for investigating the function(s) that HflX serves.

MATERIALS AND METHODS

Structural analysis of the NTD of HflX

Co-ordinates of the crystal structure of *S. solfataricus* HflX (SsHflX) was obtained from Protein Data Bank (PDB ID: 2qth) (23). This structure was analyzed to delineate domain boundaries. Coordinates of the N-terminal half (1–192 residues) were used as a query and compared against the structures in the PDB database, using DALI—online 3D structure comparison server (24). Resultant hits were manually inspected for regions of strong and weak structural similarity. Similarities that were restricted to short stretches but did not encompass an entire domain were ignored. Representative sequences of HflX were aligned by Clustal X (25), adjusted manually and analyzed for residue conservation similarly as described before (13).

Cloning expression and purification

All the clones/constructs/mutants were prepared from *E. coli* HflX and are referred with a prefix HflX in this work. HflX-WT (wild type), HflX-ΔN and HflX-ΔC were cloned expressed and purified as described previously (13). HflX-ND1 (1–120 residues) was cloned in modified *pGEX* vector (Qiagen) using 5′CGGGCGCTAGCATGT TTGACCGTTATGATGCTGG 3′ and 5′GCGGGCTCG AGCTAACCCTCATGGGTACGCGCACGTTGG 3′ as forward and reverse primers respectively, containing *NheI* and *XhoI* restriction sites. For the expression of recombinant proteins, *E. coli* BL21 cells containing the recombinant plasmid were grown at 37°C and induced with 0.1 mM IPTG (Sigma-Aldrich) at 0.6 OD measured at 600 nm wavelength. Culture was harvested by centrifugation at 4000*g* at 4°C for 10 min, after 12 h of incubation at 18°C. Cell pellet was lysed by 5 cycles of freeze-thaw in lysis buffer A [20 mM Tris–HCl (pH 8), 300 mM NaCl, 5% Glycerol, 1 mg/ml lysozyme, 3 mM β-mercaptoethanol, 1 mM PMSF, protease inhibitor cocktail (Sigma-Aldrich)]. DNase and RNase treatment followed this. Lysate thus obtained were centrifuged at 35 000*g* at 4°C for 1 h in 50 ml of oak-ridge tubes (Sorvall SS-34 rotor). Clarified supernatant was loaded on a 5 ml of Global GST-trap affinity column (Amersham) equilibrated with buffer B [50 mM Tris–HCl (pH 8.0) at 4°C, 300 mM NaCl, 5% glycerol 3 mM β-mercaptoethanol]. The column was washed with 100 ml of washing buffer B. Elution buffer (10 mM glutathione in buffer B) was used to elute the protein, and the fractions were analyzed by SDS–PAGE and concentrated with Millipore Amicon centrifugal filter tubes (10 kDa cutoff). Concentrated protein sample was further purified by size exclusion chromatography using Superdex 200 column (Amersham). Fractions containing the desired protein were concentrated using Millipore Amicon ultra centrifugation filter tubes (10 kDa cutoff), aliquoted and stored at −80°C after snap freezing in liquid nitrogen. Mutants proteins were purified using a similar protocol as described before (13).

HflX-N207A-K210A double mutant was generated by overlapping PCR technique using full-length HflX as a template. Primers were designed with the desired change in the codon sequences and are listed in Supplementary Table S1. Mutant was amplified using primers listed in Supplementary Table S1. Mutations Q28A, E29A, R114A and S32C were introduced using full plasmid amplification

with the forward and reverse primer containing mutant codons (Supplementary Table S1) using Pfu Turbo polymerase or Pfu Ultra polymerase (Stratagene). Mutations were confirmed by DNA sequencing.

Fluorescent NTP binding assays

Fluorescent nucleotide binding assays were carried out by incubating 5 μM protein with 1 μ mant-ADP or mant-GDP (fluorescent analogs of ADP and GDP) in a buffer containing 50 mM Tris–HCl (pH 8.0), 200 mM NaCl, 5 mM MgCl2, 1 mM DTT. Mant - (M N-methyl-3-O-anthranoyl) fluorescence was measured using LS-55 Fluorescence Spectrometer (PerkinElmer Life Sciences). Nucleotide binding was monitored with an excitation wavelength of 355 nm, and emission spectra were recorded in the wavelength range of 380–600 nm. Controls where the fluorescence of buffer alone, protein alone and mant-GTP/mant-ATP alone were included to assess the effect of nucleotide binding to the proteins.

GTP and ATP hydrolysis assays

GTP and ATP hydrolysis assays were carried out as described previously (13) with minor modifications. In brief, reaction was performed by incubating 10 μM HflX-WT or the other mutants of HflX with 500 μM GTP in buffer containing 50 mM Tris–HCl (pH 8.0), 200 mM NaCl, 1 mM DTT, 5 mM $MgCl_2$, 1 μCi α [^{32}P] GTP/ATP at 37°C for 60 min in 5 μl of reaction volume. The reaction was stopped by adding 1 μl of 6 M formic acid and centrifuged at 10 000 rpm for 10 min. In all, 2.5 μl of the sample was spotted on Polyethylenimine (PEI) Cellulose-coated TLC (Merck), resolved in 1.5 M KH_2PO_4 (pH 3.4) buffer and subjected to autoradiography to detect the formation of GDP/ADP. Autoradiograms were aligned with the TLC plates, and spots corresponding to GDP/ADP and GTP/ATP were cored out. The counts (CPM) were determined using scintillation counter. Background (i.e. zero time point count) was subtracted from each of the counts. Percentage hydrolysis was calculated based on the relative amount of GTP/ATP and GDP/ADP. For determining kinetic constants, 5–20 μM protein from various HflX constructs were incubated in presence of varying amount of substrate from 50 μM to 2 mM. For each concentration of substrate, rate of reaction was calculated. V_{max} and K_m was determined by Lineweaver–Burk plot (plot between 1/S and 1/V). One hour time point was chosen to determine the substrate affinity data in the Lineweaver–Burk plot.

Monitoring domain movements: DTNB reaction

The 5,5 -Dithio-bis(2-nitrobenzoic acid (DTNB) reactions with HflX mutants were carried out as described by Vopel *et al*. (26) with minor modifications. In all, 15 μM protein was incubated with 1 mM of colorless DTNB, (Invitrogen) or Ellman's reagent (27), in degassed buffer containing 50 mM Tris–HCl (pH 7.5), 200 mM NaCl, 5 mM $MgCl_2$, at 25°C. Formation of yellow thio-nitrobenzoate anion (TNB^{2-}) was detected by measuring the absorbance at 412 nm using a UV-Vis Spectrophotometer (Perkin Elmer). A cysteine residue, on reaction with DTNB, generates one molecule of TNB^{2-}. The number of reacting cysteine residues was calculated from the absorption values at 412 nm using an absorption coefficient of $\varepsilon 412 = 14150\,M^{-1}cm^{-1}$ for TNB^{2-}. Accordingly, the ordinate scale in Figure 5C was converted from absorption values to reactive cysteine equivalents.

Molecular dynamics simulations

Empirical force-field-based molecular dynamics (MD) simulations were performed on the solvated enzyme to verify domain movements in the double mutant of SsHflX, where both of the salt bridges are disrupted. Coordinates for the double mutant SsHflX were obtained from the crystal structure of the wild-type SsHflX (PDB code - 2QTH). Amino acids with the missing coordinates in the crystal structure (residues 123–143, 166–178 and 203–213) were built into it using the software *Modeler* (28). Residues E14 and E15, both were mutated to alanines *in silico* to generate the coordinates of the double mutant HflX, HflX-E14A-E15A. This double mutant was solvated with 22656 TIP3P water molecules within a periodic box of dimension $85 \times 102 \times 101$ Å^3. The system was neutralized by adding 14 Cl^- counter ions. Whole protein was treated with parm99 version of the AMBER force field (29) as available in AMBER (30). Simulations were carried out using the AMBER suite of programs. A 12 Å cutoff distance was always used while computing the non-bonded interactions. Preliminary minimization of the water molecules was followed by the minimization of the whole system. NPT simulations were carried out for 1 ns using Langevin thermostat at 300 K and Langevin barostat at 1 atm. This was followed by 5 ns NVT ensemble simulation at equilibrium volume. The time step of 1 fs was used throughout for integrating the equations of motion.

RESULTS

Recognizing a novel nucleotide-binding domain in EcHflX

To understand how HflX could satisfy ATP hydrolysis, we undertook characterization of the NTD and CTD. However, as NTD, unlike CTD, is well conserved, we focused on understanding its role; in EcHflX, this domain comprises residues 1–192. We carefully analyzed the only available structure of HflX, i.e. SsHflX from *S. solfataricus*, which is an atypical member lacking the CTD. NTD in SsHflx is 179 residues long and amino acids 166 to 179 is disordered in the available crystal structure (Figure 1) Inspecting this region suggested that NTD in SsHflX could further be divided into two distinct domains. The first domain (residues 1–98 and named ND1; for NTP-binding domain 1, see later in the text) closely resembles the Rossman fold and is made up of a centrally placed parallel β-sheet surrounded by 4 α-helices (Figure 1). The second, which we call the helical domain (HD: residues 99–165), is made up of two long α-helices. A significant part of HD (residues 123–143) is disordered in the structure of SsHflX (Figure 1). With this, EcHflX contains four domains arranged in the following order from N to C terminus: ND1-HD-ND2-CTD (Figure 2A).

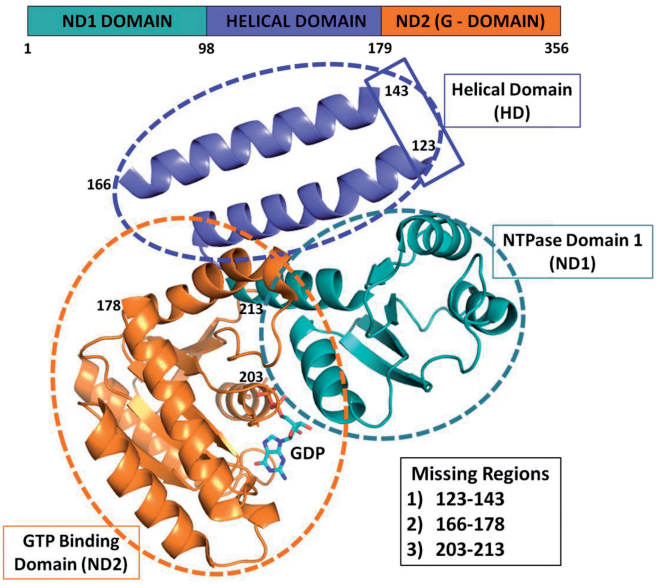

Figure 1. Domain architecture in SsHflX. The NTD is divided into two parts - ND1 (NTPase domain 1; Sea green) and HD (helical domain; violet). This is followed by the G domain or ND2 (NTPase domain 2; orange). In EcHflX, both ND1 and ND2 exhibit ATPase as well as GTPase activities and are hence termed NTPase domains. EcHflX contains an additional C terminal domain that is absent in SsHflX.

HflX was assumed to be a GTPase; further reports however suggested that it also shows significant ATP hydrolysis (13,19). To investigate whether the NTD, ND1 and/or HD may play a role in ATP binding (and/or hydrolysis), structural similarity of these with known domains in the PDB was examined using DALI—an online server for 3D structure comparison of proteins (24). ND1 displayed a poor structural similarity to the ATP-binding domain of diacyl glycerol kinase B from *Staphylococcus aureus* (DgkB, PDB ID: 2qv7) with a *Z*-score of 5 and an r.m.s.d of 2.9 Å on structurally equivalent Cα atoms (Figure 2B). This score does not reflect strong structural similarity but only indicates that a similar topology is shared by the two, i.e. a centrally placed four stranded parallel β-sheet surrounded by four α-helices (Figure 2B). Similarly, a weak structural homology could be recognized with other ATP/ADP-binding domains like malate oxidoreductase enzymes (PDB IDs—2dvm, 2hae), a hypothetical ATP-binding protein (PDB ID—1mjh), and an ATP-binding domain from a carboxylase (PDB ID—3r5h) (Supplementary Figure S7A). These provided the first clues that this domain—ND1—could be a potential ATP-binding domain and may account for ATP hydrolysis by EcHflX.

Encouraged by the structural comparisons that guide experimental investigations, here we set out to verify whether ND1 could bind and hydrolyze ATP. Toward this, a construct harboring ND1 from EcHflX (termed HflX-ND1) spanning residues 1–120 was cloned, expressed and purified. The constructs/proteins used in this study are named with a prefix HflX and imply EcHflX. Fluorescent nucleotide binding experiments using mant-ATP were used to assay for ATP binding. Comparing emission spectra 1 and 2 with 3 in Figure 2C clearly shows that HflX-ND1, like the full-length protein, binds mant-ATP. These data provide the first hint supporting a role for ND1 in ATP binding.

Further, to assess ND1's ability to hydrolyze nucleotides, GTP and ATP hydrolysis activities were assayed using radioactively labeled α[^{32}P]-GTP and α[^{32}P]-ATP and the kinetic constants, V_{max} and K_m were also determined (Figure 2D). These show that ND1 does hydrolyze ATP efficiently (Figure 2D). The kinetic parameters determined were as follows: K_m of 0.49 mM and V_{max} of 0.3 min^{-1} (Table 1). ND1 also hydrolyses GTP, but the activity is abysmally low with a V_{max}/K_m value of 0.044 $min^{-1}mM^{-1}$, when compared with 0.6 $min^{-1}mM^{-1}$ for ATP hydrolysis (Table 1). These experiments demonstrate that HflX-ND1 is largely an ATPase; however, to encompass its weak GTP hydrolysis, we have termed it an NTPase. We reasoned that creating mutant proteins in which nucleotide binding at ND2 (G-domain) in full-length HflX is abrogated would further substantiate that ND1 alone is capable of nucleotide binding/hydrolysis. Therefore, we mutated Lys210 and Asn207, present in the P-loop of the G domain (ND2), to alanines: The equivalent residues in the structure of SsHflX interact with the phosphates of GTP (23) (Supplementary Figure S1). (Asn207 also mediates an interaction with ND1 via a salt bridge N207-Q28, whose importance is discussed later). Using the mutant HflX-N207A- K210A, GTP and ATP hydrolysis activities were examined similarly. As anticipated, the ability of HflX-N207A-K210A to hydrolyze ATP was similar to that of ND1, as nucleotide binding at ND2 was abrogated. This is depicted by the V_{max}/K_m values, which are ~0.6 $min^{-1}mM^{-1}$for both HflX-ND1 and the double mutant HflX-N207A-K210A (Table 1). These data support the view that all ATP hydrolysis by the double mutant is due to ND1 alone: additionally, a control experiment was carried out using an identical double mutant generated in a construct of ND2 alone (HflX-ND2-N207A-K210A). As expected, for this mutant, ATP and GTP hydrolysis activities were completely abolished (Supplementary Figure S3).

As most GTPases and ATPases critically depend on Mg^{2+} ions for catalysis, we probed whether the ATPase activity by ND1 requires Mg^{2+}. For this, ATP hydrolysis reactions were carried out in the presence and absence of $MgCl_2$. These assays show that, like most NTPases, ND1 too requires Mg^{2+} for catalysis, and its absence abolishes most of the ATP hydrolysis activity (Figure 2E).

The double mutant HflX-N207A-K210A exhibited higher V_{max} values for GTP and ATP hydrolysis activities (0.47 ± 0.09 min^{-1} and 0.67 ± 0.01 min^{-1}, respectively), in comparison with those by ND1 alone (0.04 ± 0.010 min^{-1} and 0.3 ± 0.0026 min^{-1}, respectively) (Table 1). This possibly indicates that in the full-length protein residues other than those provided by ND1 participate in ATP/GTP hydrolysis. Similarly based on the K_m values, it may be seen that nucleotide-binding affinity too differs between ND1 and the double mutant HflX-N207A-K210A (Table 1). These comparisons warranted a critical evaluation of the contributions made by ND2

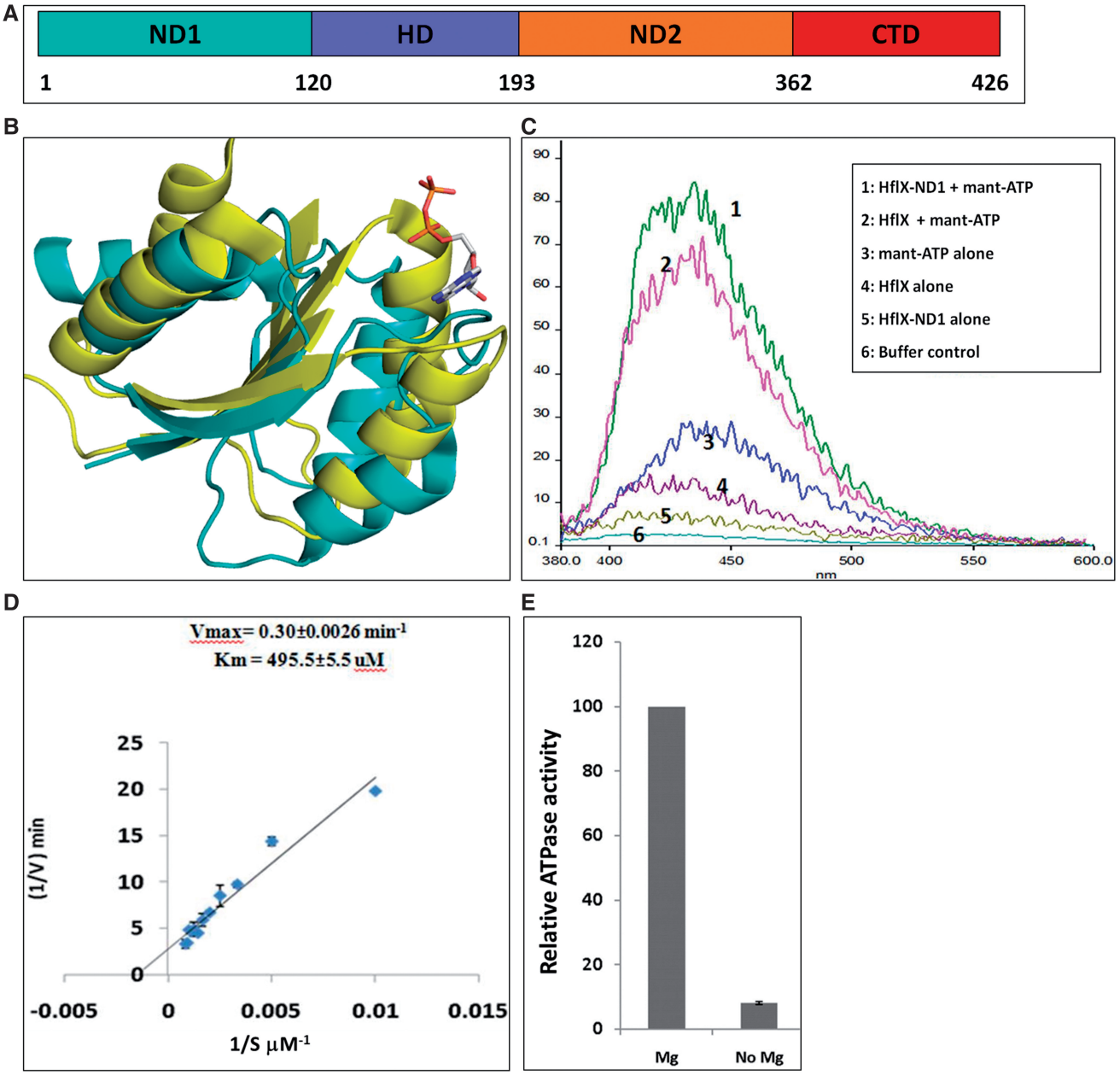

Figure 2. The N terminal domain, ND1 in HflX is an NTP binding domain. (**A**) Domain organization in EcHflX, which has an additional CTD. (**B**) ND1 of SsHflX (sea green) (2qth) is superimposed onto the ATP-binding domain of DgkB (pdb ID: 2qv7) (golden-yellow). ATP bound to DgkB is shown in sticks. (**C**) Fluorescent nucleotide binding experiments carried out for HflX (i.e. full length) and HflX-ND1 (1–120 residues) are shown. mant-ATP binding was monitored by measuring fluorescence emission [380–600 nm; 5µM protein and 1 µM mant-ATP was used]. The spectra are labeled and color-coded as indicated in the inset. (**D**) ATP hydrolysis by HflX-ND1 was measured using radiolabeled $\alpha[^{32}P]$-ATP as described in 'Materials and Methods' section. The reaction was carried out for 60 min, at varying concentrations of the substrate (S); for each concentration, rate of the reaction (V) was calculated and a Lineweaver–Burk plot (plot between 1/S and 1/V), shown on the right, was used to determine V_{max} and K_m. (**E**) ATP hydrolysis was carried out in the presence and absence of Mg^{2+} ions. EDTA was added to achieve an Mg^{2+} free state. Activity in presence of Mg^{2+} was normalized to 100%.

and other domains toward nucleotide binding and hydrolysis by ND1.

Attempts were also made to decipher the NTP-binding site in ND1. Surprisingly, the primary sequence of ND1 did not reveal a P-loop/walker-A-like feature—common to several nucleotide binding domains. Hence, structural comparisons were made with the ATP/ADP-binding proteins that were identified from DALI searches and that share a weak structural homology to ND1. A fold similar to the Rossmann fold noted in these hits and also in ND1 allowed the structural comparisons (Supplementary Material). Although the fold is similar, the structure and residues surrounding the nucleotide-binding site were variable, as evident from

Table 1. Kinetic studies of different HflX constructs were carried out as described in 'Materials and Methods' section

Construct	GTPase kinetics			ATPase kinetics		
	V_{max}/K_m ($min^{-1}mM^{-1}$)	K_m (mM)	V_{max} (min^{-1})	V_{max}/K_m ($min^{-1}mM^{-1}$)	K_m (mM)	V_{max} (min^{-1})
HflX-FL	0.36	0.839 ± 0.018	0.305 ± 0.075	1.68	0.346 ± 0.02	0.5825 ± 0.12
HflX-ND2	1.5	0.795 ± 0.079	1.20 ± 0.08	5.8	0.378 ± 0.02	2.215 ± 0.155
HflX-N207A-K210A	0.22	2.127 ± 0.31	0.47 ± 0.09	0.62	1.077 ± 0.15	0.67 ± 0.01
HflX-ND1	0.044	0.910 ± 0.13	0.04 ± 0.01	0.6	0.495 ± 0.005	0.30 ± 0.0026
HflX-ΔN	1.33	0.557 ± 0.13	0.74 ± 0.002	0.5	0.808 ± 0.107	0.41 ± 0.08
HflX-ΔC	0.188	1.862 ± 0.066	0.35 ± 0.001	0.468	1.14 ± 0.03	0.535 ± 0.014

Catalytic constants V_{max}/K_m, K_m and V_{max} values for GTPase (left half) and ATPase (right half) for each constructs are shown.
Nomenclature adopted - ND1-NTPase domain1, H-helical domain, ND2-NTPase domain 2, C-C terminal domain.

Supplementary Figure S7B. Therefore, a common site for ATP binding could not be identified from this analysis. Besides this, other *de novo* approaches were also used. These too were unsuccessful in identifying a possible ATP-binding site, as detailed in Section 1.3 'Challenges in identifying an ATP binding site in EcHflX ND1' of the Supplementary Material.

ND2 also hydrolyzes both GTP and ATP

Biochemical characterization of ND1 revealed that it hydrolyzes both GTP and ATP. To gain further insights into the nature of ND2 (the G-domain), a construct comprising ND2 alone (HflX-ND2) was generated. GTP and ATP hydrolyzing activities of HflX-ND2 were examined. The V_{max} and K_m values for GTP hydrolysis were $1.2 \pm 0.08\,min^{-1}$ and $0.795 \pm 0.079\,mM$, respectively, and those for ATP hydrolysis were $2.2 \pm 0.15\,min^{-1}$ and $0.378 \pm 0.022\,mM$, respectively. Surprisingly, ND2 appears to be catalytically more efficient in hydrolyzing ATP than GTP, as inferred from the higher V_{max}/K_m values for ATP hydrolysis (see Table 1). Interestingly, for both ATP and GTP hydrolysis, the catalytic efficiency (V_{max}/K_m) of HflX-ND2 is ~4-fold higher than that of the full-length protein (compare V_{max}/K_m values in Table 1), indicating that in all likelihood, the neighboring domains negatively regulate nucleotide binding/hydrolysis by ND2, in the full-length protein. In the absence of these, ND2 alone exhibits a higher catalytic efficiency.

Neighboring domains influence nucleotide hydrolysis by ND1 and ND2

We further sought to probe how the neighboring domains regulate the hydrolysis activity of ND1. For this, we systematically determined the kinetic constants (for ATP, GTP hydrolysis separately) for constructs lacking one domain at a time (see Table 1). Indeed, we could identify a regulation imposed by the neighboring domains. To evaluate the influence of NTD (henceforth, referred as ND1 + HD), a deletion construct of EcHflX devoid of ND1 + HD (residues 1–192), i.e. HflX-ΔN was generated. Kinetic constants K_m and V_{max} were similarly determined. The K_m ($0.557 \pm 0.136\,mM$) and V_{max} ($0.74 \pm 0.02\,min^{-1}$) values for GTP hydrolysis by HflX-ΔN are comparable with those for HflX-ND2, i.e. ND2 domain in isolation (see Table 1). This also implies that like HflX-ND2, HflX-ΔN also exhibits ~4-fold higher efficiency as compared with full-length in hydrolyzing GTP. Put together, these clearly imply that in the full-length protein, ND1 + HD render an inhibitory effect on the GTP hydrolysis of ND2 (Figure 3A). These results are in concordance with studies on SsHflX, where a similar increase in activity was observed on deleting ND1 + HD (23).

The kinetic constants K_m and V_{max} for ATPase activity by HflX-ΔN were $0.808 \pm 0.107\,mM$ $0.41 \pm 0.08\,min^{-1}$, respectively. The catalytic efficiency, i.e. V_{max}/K_m was $0.5\,min^{-1}mM^{-1}$, which is 1/10th that of ND2 in isolation, i.e. HflX-ND2 (also compare the V_{max} values, Table 1). As HflX-ΔN also contains the CTD in addition to ND2, this comparison should imply that CTD inhibits ATP hydrolysis by ND2 (Figure 3B). However, a similar inhibition of GTP hydrolysis by CTD is not evident (Figure 3A).

To verify the influence by CTD, we generated a deletion construct, HflX-ΔC, devoid of CTD (lacking 64 residues, i.e. 363–426, at the C-terminus). Based on kinetic data presented in Table 1, deleting CTD seems to influence GTP and ATP hydrolysis activities, (depicted schematically in Figure 3). While comprehending its precise influence on the hydrolysis activities of ND1 and ND2 individually appears complex, based on kinetics data, it appears that deleting CTD affects nucleotide binding rather than rate of the reaction (Table 1).

In summary, it suffices to conclude that CTD plays an important regulatory role for ATP hydrolysis (Figure 3B). Given this, it is intriguing that CTD is absent in some of the HflX homologues. Interestingly, SsHflX and CpHflX (from *Chlamydophilla pneumonia*), which both lack the CTD, are also devoid of ATPase activity (14,31). In the absence of crystal structures of HflX proteins that contain CTD, and as only a few (HflX) homologues have been characterized comprehensively, gauging the precise nature of this regulation mediated by the CTD would be difficult.

Two salt bridges regulate hydrolysis activities of ND1 and ND2

Although the structure of SsHflX, devoid of CTD would limit evaluating the regulation by the CTD, it would allow

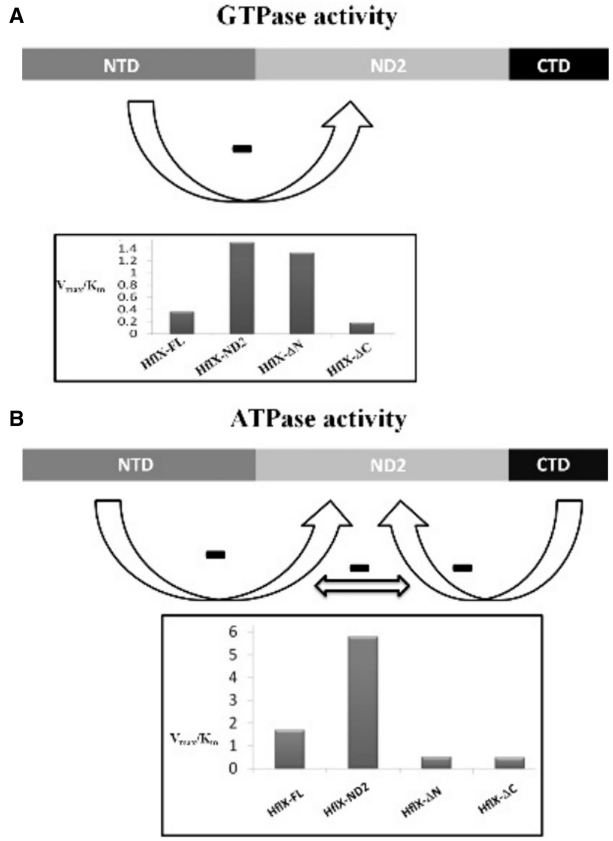

Figure 3. Schematic representation of the influence of the neighboring domains on the catalytic activities. (**A**) Effect of neighboring domains on the GTPase activity in EcHflX. NTD (ND1 + HD) negatively regulates (negative regualtion depicted by '-' sign) the GTPase activity of ND2. This is deduced based on the higher catalytic efficiency, V_{max}/K_m of HflX-ND2 (i.e. ND2 alone) as compared with that of HflX-ΔC (in which NTD and ND2 are present); compare efficiencies of these in the inset. A higher catalytic efficiency of HflX-ΔN as compared with HflX-FL also emphasizes the inhibitory role played by NTD. Compare efficiencies of these in the inset and see Table 1. (**B**) Influence of neighboring domains on the ATPase activity in EcHflX. NTD (ND1 + HD) negatively regulates (depicted by '-' sign) ATP hydroysis by ND2 as inferred from a higher activity by HflX-ND2 (i.e. ND2 alone) than by HflX-ΔC (which has NTD and ND2). Compare V_{max}/K_m of HflX-ND2 versus HflX-ΔC in the inset (also shown in Table 1). Similarly, CTD also negatively regulates ATP hydroysis of ND2 as inferred from a higher efficiency of HflX-ND2 than that of HflX-ΔN (which has ND2 and CTD). Compare these values in the inset. Furthermore, NTD and CTD appear to oppose each other's inhibition and lead to an increased efficiency in HflX-FL, as compared with HflXΔC and HflX-ΔN, but not HflX-ND2 (compare V_{max}/K_m values of HflX-FL versus HflX-ΔC and HflX-ΔN in the inset and Table 1). However, ND2 alone (HflX-ND2) possesses the highest activity. Also note the relative difference in efficiencies for GTP and ATP hydrolysis, indicating HflX is a better ATPase.

comprehending the influence by ND1 + HD. It was previously reported that ND2, the typical G domain, has a GTP binding site in a cleft facing ND1 (Figure 1) and the presence of three interactions that seem to fasten ND1 and ND2 together across this cleft (22) (Supplementary Figure S2). This too suggests that ND1 + HD may influence the catalytic activity of EcHflX. The kinetics data for the constructs lacking ND1 + HD clearly suggest that it plays a regulatory role, where in it inhibits GTP and ATP hydrolysis by the full-length protein (Table 1, Figure 3).

Three stabilizing interactions in SsHflX seems to fasten the two domains, ND1 and ND2 together: these are (i) the carboxyl group of D232 (of ND2) that interacts with H97 (from ND1); (ii) the amino group of N189 (from ND2) that interacts with the carboxyl group of E14 (of ND1) and (iii) the amino group of R238 (from ND2) that interacts with carboxyl group of E15 (of ND1) (Supplementary Figure S2). Although the first and third are electrostatic interactions or salt bridges, the second is a hydrogen bond. However, for ease of presentation, we refer to all of these as salt bridges. To map these interactions in EcHflX, we generated a homology model based on the structure of SsHflX. A superposition of the two resulted in an root mean square deviation (r.m.s.d.) of 0.172, for 1077 backbone atoms. The salt bridges aforementioned would correspond to R114-D251, E29-R257 and Q28-N207 in EcHflX (Figure 4B). To assess their importance for ND1 and ND2, we disrupted them one at a time, by mutating one of the residues constituting a salt bridge. The mutants HflX-R114A, HflX-E29A and HflX-Q28A in EcHflX would thus disrupt the three salt bridges R114-D251, E29-R257 and Q28-N207, respectively. The salt-bridge disrupting mutants were generated, and mutant proteins, purified to homogeneity, were assayed for their ability to hydrolyze ATP and GTP.

The ATP and GTP hydrolysis of HflX-R114A was found comparable with HflX-WT (Supplementary Figure S4A). Interestingly, the ATPase activity of HflX-E29A was ~5-fold higher than HflX-WT, whereas its GTPase activity was similar (Figure 4C). In contrast, for HflX-Q28A both GTP and ATP hydrolysis increased by ~3-fold (compared with HflX-WT). Thus, amongst the three interactions identified at the interface, two were found to have regulatory effects on the nucleotide hydrolysis activities in HflX. To see the combined effect of disrupting both of the salt bridges, a double mutant, HflX-Q28A-E29A was created. Although qualitative, it appears that the increase in GTPase and ATPase activities seen for this mutant shows an almost additive effect of the activities of the single mutants HflX-Q28A and HflX-E29A (Figure 4C).

Mutations Q28A and E29A enhance ATPase and/or GTPase activities. To further inquire whether the increase in activities are associated with a change in nucleotide binding, fluorescence nucleotide binding assays were performed by incubating fluorescently labeled mant-ADP and mant-GDP with HflX-WT and mutant proteins. In separate experiments, when the mutant HflX-Q28A was incubated with mant-ADP and with mant-GDP, an increase in fluorescence was observed as compared with the HflX-WT (Figure 4D and E). This suggests a better binding of ATP and GTP by HflX when the interaction Q28-N207 is disrupted. In contrast, for the mutant HflX-E29A, an increase in fluorescence was observed (in comparison with HflX-WT) with mant-ADP but not with mant-GDP (Figure 4D and E). On the other hand, the double mutant HflX-Q28A-E29A displays a higher binding for both GTP and ATP than either of the single mutants. Similar nucleotide binding experiments

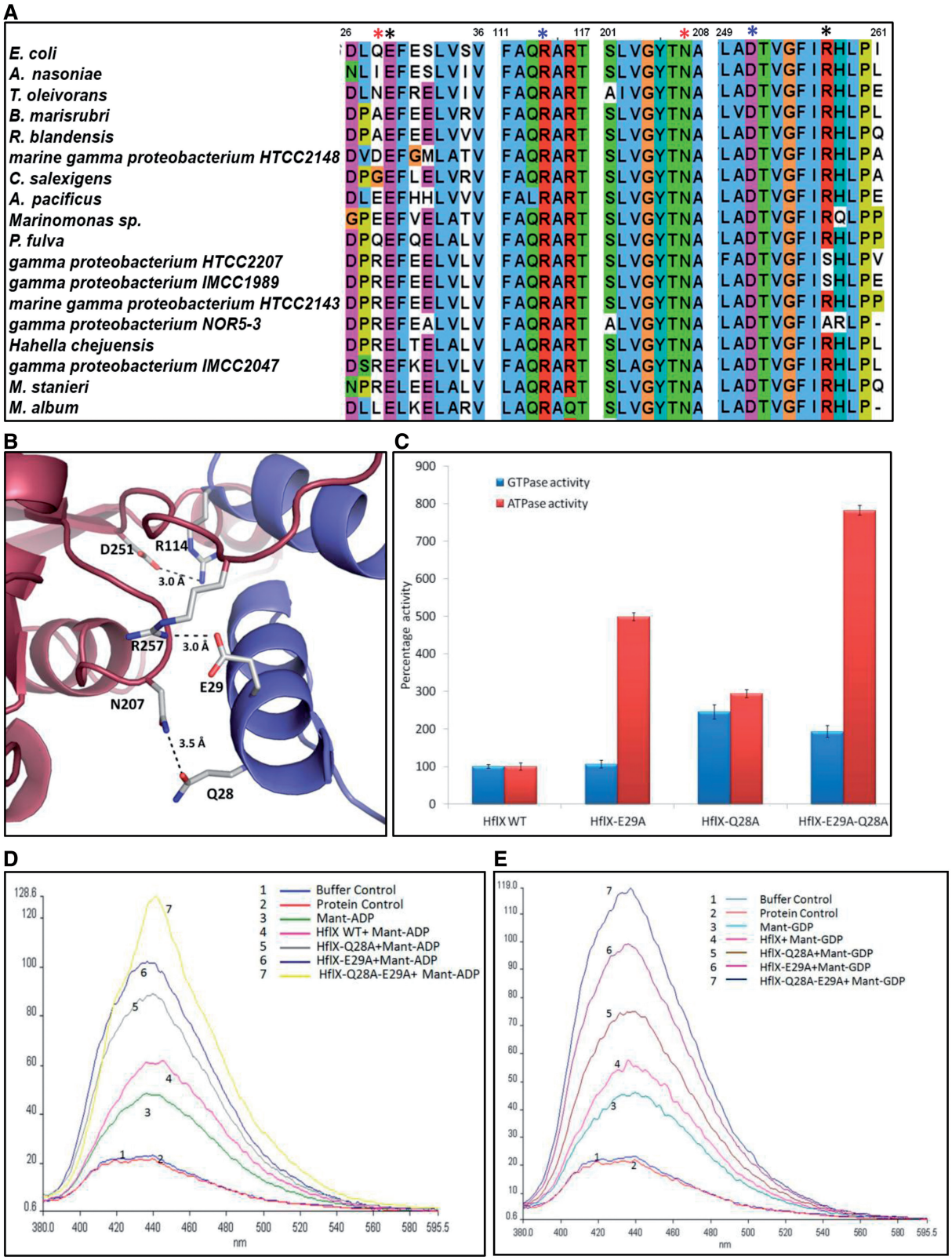

Figure 4. Two salt bridges Q28-N207 and E29-R257 regulate GTPase and ATPase activities of EcHflX. (**A**) Residues constituting the salt bridges R114-D251 (blue asterisks), E29-R257 (black asterisks) and N207-Q28 (red asterisks) are shown in the multiple sequence alignment of representative HflX homologues (the corresponding gi numbers may be found in Supplementary Material). Numbers on the top (correspond to EcHflX) indicate regions containing these residues. Of these, E29, R114, D251, R257 and N207 are conserved among the HflX homologues. Q28 (first red asterisk from left) is not strictly conserved but is often a residue capable of forming a hydrogen bond via–OH group. (**B**) Interactions R114-D251, Q28-N207 and E29-R257 between ND2 (brown-red) and the ND1 (purple) in the homology model of EcHflX are shown. Disrupting the salt bridge R114-D251 did not affect ATP/GTP hydrolysis activities by EcHflX (see Supplementary Figure S4). (**C**) GTP (blue) and ATP (red) hydrolysis activities by

(continued)

with HflX-R114A mutant did not show any appreciable increase in nucleotide binding (S4B-C). Although qualitative, these experiments indicate that the differences in GTPase/ATPase activities arise due to altered nucleotide binding by the mutants. Altogether, these data suggest that the salt bridges, E29-R257 and Q28-N207, contribute to inter-domain regulation and affect nucleotide hydrolysis activities at ND1 and ND2.

Disruption of the salt bridge E29-R257 unfastens ND1-ND2 interface and triggers domain movement

It appears that the two salt bridges fastening ND1 and ND2 regulate nucleotide binding and thus their hydrolysis activities. We envisaged that this might be achieved via domain movements, triggered due to the disruption of the salt bridge(s). Also, we reasoned that in the wild-type protein, these salt bridges may be affected following ribosome binding, as the interaction of 50S ribosomal subunits with HflX is known to enhance its GTPase activity (13).

Overall, it appeared reasonable to anticipate domain movements in HflX. To examine this, an indirect method that detects exposed cysteine residues was used (27). This method uses Ellman's reagent DTNB, which interacts with the thiol group of exposed cysteine(s) to produce a colored complex, which absorbs light at 412 nm. Based on the absorbance, the number of exposed cysteine residues can be estimated. This method was exploited to gauge domain movements in HflX. However, an analysis of the structure of SsHflX did not identify any buried cysteines at the ND1-ND2 interface. Therefore, other residues that could be mutated to a cysteine were identified and then used in the aforesaid experiment to monitor domain movements. One such residue identified in EcHflX at the ND1-ND2 interface was Ser32 (corresponds to Ala18 in SsHflX), which was largely conserved, buried and was close to the GTP binding site (Figure 5A and B). Hence, it was mutated to a Cys. Stability of HflX-S32C mutant protein was also confirmed by examining its nucleotide hydrolysis activity, which was almost similar to HflX-WT (Supplementary Figure S6). Therefore, S32C mutation was introduced together with the salt bridge disrupting mutations such that the exposure of Cys32 on disrupting the two salt bridges could be probed; if exposed, it would indicate the opening of the ND1-ND2 interface. In essence, domain movements were examined by using HflX-WT, mutants HflX-S32C, HflX-S32C-E29A, HflX-S32C-Q28A and HflX-S32C-E29A-Q28A in the DTNB reactions, aforementioned.

As anticipated, in these, HflX-WT does not show that a cysteine is exposed. HflX-S32C mutant too behaves similarly, indicating the Cys at 32 is buried at the interface (Figure 5C). However, in the HflX-S32C-E29A mutant, one cysteine is exposed, suggesting that the disruption of E29-R257 exposes the otherwise buried Cys32 that reacts with DTNB to produce the yellow colored complex (Figure 5C). In contrast, when the mutant HflX-S32C-Q28A was used in these assays, a similar effect, i.e. the exposure of Cys32, could not be noticed (Figure 5C), indicating that the disruption of Q28-N207 is not sufficient to cause domain movements that enable the exposure of Cys32. However, in the triple mutant HflX-S32C-E29A-Q28A, where both salt bridges are disrupted, exposure of Cys32 could be observed once again (Figure 5C).

This is in contrast to the observation that nucleotide binding increases when either of the salt bridges is disrupted. Therefore, it could be that domain movement involving an alternative surface, away from Cys32, occurs in the mutant HflX-Q28A, and these could not be monitored in the current experiment.

To further gauge domain movements in the protein, an MD simulation study was carried out using SsHflX, where E14 and E15 corresponding to Q28 and E29 of EcHflX were mutated to alanines. This simulation, run for 5 ns, demonstrated movements in ND1 and ND2; here, the r.m.s.d. value observed between the initial and the final positions of the protein (backbone) atoms was 3.57 Å. This value is indicative of a large structural variation. Figure 5D shows the change in the structures of SsHflX during the simulation; it shows the initial, intermediate and final frames (after 5 ns simulation)—colored red, white and blue, respectively. The individual domains ND1, ND2 and HD show negligible change in domain architecture during the entire course of the simulation. However, this difference evaluated for the entire molecule depicts higher r.m.s.d. values, indicating significant changes in the positions of the domains. In particular, and as inferred from experiments, it depicts an opening of the ND1-ND2 interface (compare red and blue ribbons, Figure 5D). A preliminary analysis of the interface of ND1 and ND2 in Supplementary Figure S6 depicts how the unfastening of two domains occurs and results in the exposure of Ala18 (equivalent to S32 in EcHflX, which was mutated to cys in the aforesaid experiments). For this analysis, 10 pairs of residues at the interface of ND1 and ND2 were identified; in each pair, one residue was from ND1 and another in the closest vicinity was from ND2. For each pair of residues, the initial distance between their Cα atoms (D1) was compared with the final distance between the same pair of Cα atoms (D2), i.e. at the end of the 5 ns simulation. Based on the difference ΔD (= D2-D1) for each pair of residues, a possible means by which the domains open could be inferred (Supplementary Figure S6). As shown in

Figure 4. Continued
HflX-WT and mutants HflX-Q28A and HflX-E29A are shown. Activity of HflX-WT was normalized to 100%. (**D** and **E**) Ability of HflX mutants to bind fluorescently labeled nucleotides, mant-ADP (D) and mant-GDP (E) was assessed by comparing fluorescence emission (arbitrary units) by the mant group in the presence and absence of the proteins, similarly as in Figure 2C. The inset shows the spectra recorded for the various constructs and are demarcated by corresponding numbers. Buffer control indicates only the buffer was present, and protein control implies the free protein (without mant-nucleotides).

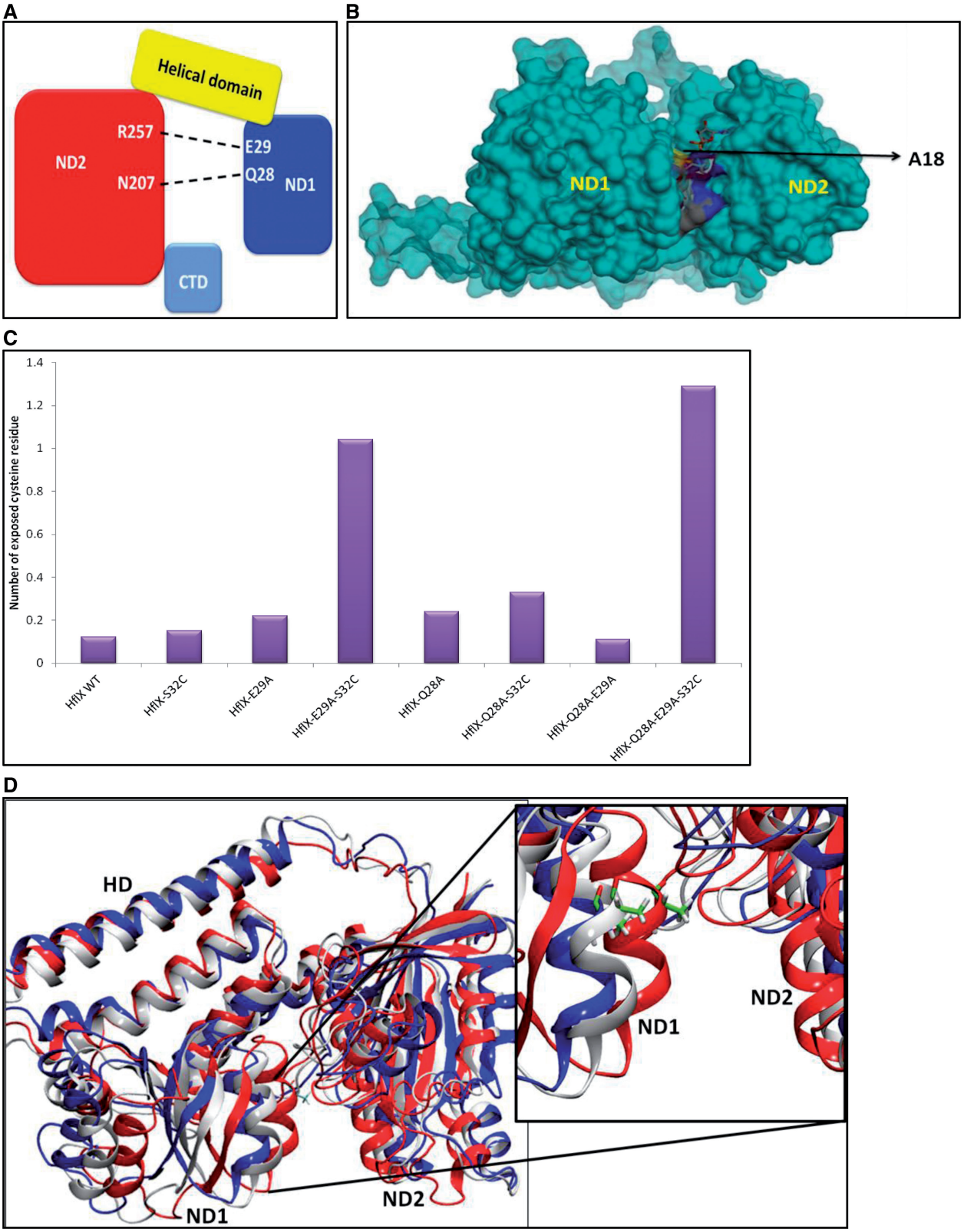

Figure 5. E29A mutation in HflX is associated with the opening of a cleft between domains ND1 and ND2, as inferred by the exposure of an otherwise buried cysteine. (**A**) A schematic of domains in HflX is shown. Two salt bridges E29-R257 and Q28-N207 (indicated by dashed line) that affect the activities of ND1 (blue) and ND2 (red) are shown; these two domains are connected by a helical domain (yellow) that likely binds the ribosome. (**B**) A surface representation of SsHflX showing Ala18 buried at the interface of ND1 and ND2; the equivalent residue Ser32 in EcHflX was mutated to cysteine to create HflX-S32C mutant. (**C**) The proteins indicated on the *X*-axis of the histogram were incubated with DTNB, and the number of exposed cysteine residues, calculated as described in the 'Materials and Methods' section, is shown on the *Y*-axis. (**D**) MD simulations were run for 5 ns to gauge domain movements in HflX. A trajectory of domain movements in SsHflX during NVT simulation was obtained, of which

(continued)

Supplementary Figure S6, regions closer to the helical domain show lesser ΔD, whereas those on the opposite end show higher ΔD. Tracing ΔD from smaller to larger values provides the extent of domain opening along the interface (shown by an arrow in Supplementary Figure S6). Interestingly, of the three salt bridges at the interface, salt bridges E29-R257 and Q28-N207 that affect the activities of ND1 and ND2, lie at the region that shows a high ΔD, i.e. larger domain unfastening. On the other hand, the interaction R114-D251 lies at the region that depicts minimal domain opening. This possibly explains why disrupting R114-D251 interaction did not alter nucleotide binding and hydrolysis.

DISCUSSION

HflX is a multi-domain ribosome binding GTPase whose precise cellular function is to be established. Previously, it was believed to be involved in lytic-lysogeny decision, but this role was negated by Dutta *et al*. (19). Simultaneously, we showed that it binds the ribosome and may hence be involved in its biogenesis (13). An intriguing feature identified in both the studies was that HflX, besides hydrolyzing GTP also hydrolyzes ATP; in this work, we show that it has a better catalytic efficiency to hydrolyze ATP than GTP. The current study is aimed at further clarifying these activities of HflX and identifying the region responsible for ATP binding. A weak structural homology to a few of the ATP-binding domains, including that of DgkB, prompted us to investigate whether the N terminal region possessed an ATP-binding domain. Indeed, biochemical studies presented here confirm ND1 to be a new ATP-binding domain in HflX, which largely hydrolyzes ATP, with feeble GTPase activity. Unlike the conventional GTP/ATP-binding domains, ND1 does not contain a P-Loop/walker-A motif: ttempts to identify the nucleotide binding site in ND1 appears demanding and likely requires the structure of ND1 (or full-length HlfX) bound to ATP/GTP (see 'Challenges in identifying an ATP binding site in EcHflX ND1' in the Supplementary Material).

Another surprising finding is that the G-domain (ND2) too hydrolyzes ATP as well as GTP; moreover, it is atypical that it hydrolyzes ATP more efficiently. ATP is hydrolyzed more efficiently by ND2 than by ND1 (V_{max}/K_m values: 5.8 $min^{-1}mM^{-1}$ versus 0.6 $min^{-1}mM^{-1}$) when measured in isolation. In full-length HflX, these activities may be distributed differently due to the interplay between the neighboring domains, which seems to be complex. Furthermore, both the domains adjacent to ND2, i.e. ND1 and CTD, appear to suppress its ATPase activity, whereas the GTPase activity seems to be regulated only by ND1 (Figure 3). Evidently, picturing complex regulation such as this would require extensive investigations.

Nevertheless, a ramification of the finding that ND1 hydrolyzes ATP and GTP is that all HflX proteins must possess this activity, as ND1 is common to all HflX homologues. However, as SsHflX and CpHlfX were not found to possess ATPase activity, it could either be that ND1 (and ND2) in these proteins has specificity for GTP alone (i.e. SsHflX and CpHlfX like homologues do not possess the ability to bind ATP); ND1 is inactive in a subset of HflX homologues like these. Is nucleotide specificity tailored for a specific role in certain homologues? Extensive investigations along these lines, involving several (and distinct) HflX homologues, would be required before attempting to address such questions.

In HflX, ND1 and ND2 interact via three salt bridges, which seem to clutch the two domains together. These salt bridges were disrupted one at a time and two of these, Glu29-Arg257 and Gln28-Asn207, appear to regulate the activities of ND1 and ND2. When the first was disrupted due to the mutation E29A, the ATPase activity increased by 5-fold compared with that of HflX-WT, whereas the GTPase activity remained unchanged (Figure 4C). This suggests that Glu29-Arg257 serves as a clamp holding ND1 and ND2 in close proximity; this fastening of the two domains appears to inhibit ATP hydrolysis. Gaining a better insight into how this salt bridge regulates ATP hydrolysis in the two domains necessitates locating the ATP binding site(s) in ND1 and ND2; future studies should be aimed at determining this. Similarly, disrupting the second salt bridge (due to Q28A) increased both GTP and ATP hydrolysis activities of HflX-Q28A by ~3-fold (compared with that by HflX-WT) (Figure 4C). In the double mutant, HflX-Q28A-E29A (where both the salt bridges are disrupted), the increase in GTPase and ATPase activities shows an almost additive effect of the effects seen for the single mutants HflX-Q28A and HflX-E29A (Figure 4C). Would this imply that the two salt bridges regulate the two activities independently? Again, future studies should address these aspects. Overall, interdomain regulations mediated by the two salt bridges appear critical to the function of HflX.

Domain deletion studies presented here indicate that ND1 + HD inhibit the activity of ND2 (Table 1). Similar inhibition was also observed in SsHflX (23). On disrupting two salt bridges, a higher NTPase activity increased nucleotide binding and the exposure of a buried cysteine indicating larger domain movements are observed. These observations indicate that the inhibition caused by the neighboring domains is released probably due to an opening of the cleft between ND1 and ND2, which is the GTP-binding site. Hence, this opening appears to result in increased NTP binding and its hydrolysis; this may serve as a plausible model explaining inter-domain regulation in the protein. MD simulations presented here also depict extensive domain movements in this protein.

Figure 5. Continued
conformations at three different stages of the simulation are shown. Red colored ribbon represents the initial protein conformation, white ribbon represents an intermediate frame in the trajectory and blue cartoon represents the conformation in the last frame at the end of 5 ns simulation. The inset shows how the domain opening would expose Ala18 (the corresponding S32 in EcHflX was mutated to a cysteine), which was initially buried at the interface of ND1 and ND2. Ala18 is shown as sticks (carbon atoms are green and hydrogen atoms are white).

The identification of a novel NTP-binding site (ND1) in HflX provides the scope to revisit the inferences drawn in a few recent reports. A recent study describing kinetic studies on *E. coli* HflX reported that both GTP and ATP hydrolysis are stimulated on binding with 50S and 70S ribosomal subunits (18). However, they concluded EcHflX to be a GTP-binding protein and not an ATP-binding protein, based on the affinities measured for GTP and ATP. These studies assumed one common site (i.e. at ND2) for binding both GTP and ATP. The affinities for the nucleotides were measured based on a FRET signal between the florescent mant group of the nucleotides used in these studies and a tryptophan residue present around the nucleotide-binding site in ND2. A FRET signal noted for ATP binding was much lower than for GTP binding, which led the authors to conclude that HflX would adopt an alternative conformation when bound to ATP. In contrast, our study by considering two independent sites (i.e. ND1 and ND2) for nucleotide binding provides the following alternative view: In the current situation, ATP could bind both ND1 and ND2, unless binding to either is negatively influenced/inhibited in the full-length protein owing to interdomain interactions. If ATP binds the identical site as GTP in ND2, a strong FRET signal should have been observed, but this is not the case. Here, we demonstrate that ND2 binds ATP efficiently. Hence, this raises the possibility that ATP binds differently (in a manner that it does not evoke a strong FRET signal) at the same site or binds at a different site in ND2. Therefore, it seems reasonable to suggest that ATP binds at ND1 in the full-length protein, albeit with a poor binding affinity. The absence of a tryptophan in this region at ND1 would further explain the smaller FRET signal when ATP binding was assayed by Shields *et al.* (21). Further studies would be needed to understand how ATP binds at ND2. For this, a construct of HflX with completely abolished nucleotide binding at ND1 would be required, and at present, the challenges in identifying the nucleotide-binding site in ND1 pose a limitation. Furthermore, another report by Fischer *et al.* (15) showed that in pre-steady-state kinetics analysis, GDP binding to EcHflX occurs in two steps with different equilibrium constants. Following the characterization of ND1, this may be reinterpreted as binding of GDP to the two independent binding sites in ND1 and ND2.

We infer a conformational change leading to the opening of the cleft formed by domains ND1 and ND2. This is based on the exposure of an otherwise buried cysteine following the disruption of the salt bridge E29-R257. ND1 and ND2 are linked by the domain HD, which has two helices connected by a long glycine rich linker (residues 123–143 in SsHflX), which is disordered in the crystal structure of SsHflX (Figure 1). Based on the presence of several positively charged solvent exposed amino acids, it appears that HD probably interacts with rRNA via these residues. HflX is known to bind ribosomal subunits. It is possible to envisage a scenario where this binding at HD likely stimulates a conformational change similar to the one inferred on disrupting the salt bridges aforementioned. Albeit speculative, this might be a probable mechanism relating ribosome binding to a stimulated NTP hydrolysis in HflX; at least this proposal would trigger investigations in this direction. With the identification of two NTPase domains in HflX, a more complex regulation with respect to the biological function of HflX may be anticipated. We had previously shown an intricate domain–domain interaction between two guanine nucleotide binding domains (GD1 and GD2) in EngA, which allows EngA to switch between two ribosome bound states—one where it only binds 50S and another where it binds 50S, 30S and 70S ribosomal subunits (12). These two states of EngA are realized when GD1 and GD2 adopt different nucleotide bound states. Hitherto, HflX too was known to bind 50S alone. Recently, it was shown to bind 50S, 30S and 70S subunits (15). A similar and perhaps more complex regulation should be expected for HflX, as ND1 and ND2 can bind and hydrolyze two different nucleotide bases (adenine and guanine) unlike the GTP binding domains in EngA that are specific to guanine nucleotides. Several combinations can be anticipated for ND1 and ND2 in HflX, as each of them can exist in four possible states, bound to ATP/ADP/GTP/GDP. Future work should reveal interesting structure–function relationships in HflX, particularly with regard to its role in ribosome biogenesis.

SUPPLEMENTARY DATA

Supplementary Data are available at NAR Online.

ACKNOWLEDGEMENTS

The authors thank Drs Vinay Nandicoori and Nisanth N. Nair for valuable discussions; Navdeep Yadav and Deepak Joshi for technical help. They thank M. Saravanan for inputs and efforts toward identifying a likely ATP-binding site in ND1. N.J. acknowledges CSIR, India for financial support in the form of an SRF (senior research fellowship).

FUNDING

Department of Science and Technology, India; Department of Biotechnology, India and Council of Scientific and Industrial Research. Funding for open access charge: Indian Institute of Technology, Kanpur (partial).

Conflict of interest statement. None declared.

REFERENCES

1. Leipe,D.D., Wolf,Y.I., Koonin,E.V. and Aravind,L. (2002) Classification and evolution of P-loop GTPases and related ATPases. *J. Mol. Biol.*, **317**, 41–72.
2. Britton,R.A. (2009) Role of GTPases in bacterial ribosome assembly. *Ann. Rev. Microbiol.*, **63**, 155–176.
3. Matsuo,Y., Morimoto,T., Kuwano,M., Loh,P.C., Oshima,T. and Ogasawara,N. (2006) The GTP-binding protein YlqF participates in the late step of 50 S ribosomal subunit assembly in Bacillus subtilis. *J. Biol. Chem.*, **281**, 8110–8117.

4. Uicker,W.C., Schaefer,L. and Britton,R.A. (2006) The essential GTPase RbgA (YlqF) is required for 50S ribosome assembly in Bacillus subtilis. *Mol. Microbiol.*, **59**, 528–540.
5. Sato,A., Kobayashi,G., Hayashi,H., Yoshida,H., Wada,A., Maeda,M., Hiraga,S., Takeyasu,K. and Wada,C. (2005) The GTP binding protein Obg homolog ObgE is involved in ribosome maturation. *Genes Cells*, **10**, 393–408.
6. Muench,S.P., Xu,L., Sedelnikova,S.E. and Rice,D.W. (2006) The essential GTPase YphC displays a major domain rearrangement associated with nucleotide binding. *Proc. Natl Acad. Sci. USA.*, **103**, 12359–12364.
7. Schaefer,L., Uicker,W.C., Wicker-Planquart,C., Foucher,A.E., Jault,J.M. and Britton,R.A. (2006) Multiple GTPases participate in the assembly of the large ribosomal subunit in Bacillus subtilis. *J. Bacteriol.*, **188**, 8252–8258.
8. Sharma,M.R., Barat,C., Wilson,D.N., Booth,T.M., Kawazoe,M., Hori-Takemoto,C., Shirouzu,M., Yokoyama,S., Fucini,P. and Agrawal,R.K. (2005) Interaction of Era with the 30S Ribosomal Subunit: Implications for 30S Subunit Assembly. *Mol. Cell*, **18**, 319–329.
9. Kimura,T., Takagi,K., Hirata,Y., Hase,Y., Muto,A. and Himeno,H. (2008) Ribosome-small-subunit-dependent GTPase interacts with tRNA-binding sites on the ribosome. *J. Mol. Biol.*, **381**, 467–477.
10. Anand,B., Surana,P., Bhogaraju,S., Pahari,S. and Prakash,B. (2009) Circularly permuted GTPase YqeH binds 30S ribosomal subunit: implications for its role in ribosome assembly. *Biochem. Biophys. Res. Commun.*, **386**, 602–606.
11. Anand,B., Surana,P., Bhogaraju,S., Pahari,S. and Prakash,B. (2009) Circularly permuted GTPase YqeH binds 30S ribosomal subunit: Implications for its role in ribosome assembly. *Biochem. Biophys. Res. Commun.*, **386**, 602–606.
12. Tomar,S.K., Dhimole,N., Chatterjee,M. and Prakash,B. (2009) Distinct GDP/GTP bound states of the tandem G-domains of EngA regulate ribosome binding. *Nucleic Acids Res.*, **37**, 2359–2370.
13. Jain,N., Dhimole,N., Khan,A.R., De,D., Tomar,S.K., Sajish,M., Dutta,D., Parrack,P. and Prakash,B. (2009) E. coli HflX interacts with 50S ribosomal subunits in presence of nucleotides. *Biochem. Biophys. Res. Commun.*, **379**, 201–205.
14. Blombach,F., Launay,H., Zorraquino,V., Swarts,D.C., Cabrita,L.D., Benelli,D., Christodoulou,J., Londei,P. and van der Oost,J. (2011) An HflX-type GTPase from Sulfolobus solfataricus binds to the 50S ribosomal subunit in all nucleotide-bound states. *J. Bacteriol.*, **193**, 2861–2867.
15. Fischer,J.J., Coatham,M.L., Eagle Bear,S., Brandon,H.E., De Laurentiis,E.I., Shields,M.J. and Wieden,H.J. (2012) The ribosome modulates the structural dynamics of the conserved GTPase HflX and triggers tight nucleotide binding. *Biochimie*, **94**, 1647–1659.
16. Bourne,H.R., Sanders,D.A. and McCormick,F. (1990) The gtpase superfamily - a conserved switch for diverse cell functions. *Nature*, **348**, 125–132.
17. Sigal,I.S., Gibbs,J.B., D'Alonzo,J.S., Temeles,G.L., Wolanski,B.S., Socher,S.H. and Scolnick,E.M. (1986) Mutant ras-encoded proteins with altered nucleotide binding exert dominant biological effects. *Proc. Natl Acad. Sci.*, **83**, 952–956.
18. Wittinghofer,A. and Pal,E.F. (1991) The structure of Ras protein: a model for a universal molecular switch. *Trends Biochem. Sci.*, **16**, 382–387.
19. Dutta,D., Bandyopadhyay,K., Datta,A.B., Sardesai,A.A. and Parrack,P. (2009) Properties of HflX, an Enigmatic Protein from *Escherichia coli*. *J. Bacteriol.*, **191**, 2307–2314.
20. Koller-Eichhorn,R., Marquardt,T., Gail,R., Wittinghofer,A., Kostrewa,D., Kutay,U. and Kambach,C. (2007) Human OLA1 Defines an ATPase Subfamily in the Obg Family of GTP-binding Proteins. *J. Biol. Chem.*, **282**, 19928–19937.
21. Shields,M.J., Fischer,J.J. and Wieden,H.J. (2009) Toward understanding the function of the universally conserved GTPase HflX from *Escherichia coli*: a kinetic approach. *Biochemistry*, **48**, 10793–10802.
22. Wu,H., Sun,L., Blombach,F., Brouns,S.J., Snijders,A.P., Lorenzen,K., van den Heuvel,R.H., Heck,A.J., Fu,S., Li,X. *et al.* (2010) Structure of the ribosome associating GTPase HflX. *Proteins*, **78**, 705–713.
23. Wu,H., Sun,L., Blombach,F., Brouns,S.J.J., Snijders,A.P.L., Lorenzen,K., van den Heuvel,R.H.H., Heck,A.J.R., Fu,S., Li,X. *et al.* Structure of the ribosome associating GTPase HflX. *Proteins*, **78**, 705–713.
24. Holm,L. and Rosenström,P. (2010) Dali server: conservation mapping in 3D. *Nucleic Acids Res.*, **38**, W545–W549.
25. Larkin,M.A., Blackshields,G., Brown,N.P., Chenna,R., McGettigan,P.A., McWilliam,H., Valentin,F., Wallace,I.M., Wilm,A., Lopez,R. *et al.* (2007) Clustal W and Clustal X version 2.0. *Bioinformatics*, **23**, 2947–2948.
26. Vopel,T., Kunzelmann,S. and Herrmann,C. (2009) Nucleotide dependent cysteine reactivity of hGBP1 uncovers a domain movement during GTP hydrolysis. *FEBS Lett.*, **583**, 1923–1927.
27. Ellman,G.L. (1959) Tissue sulfhydryl groups. *Arch. Biochem. Biophys.*, **82**, 70–77.
28. Fiser,A., Do,R.K. and Sali,A. (2000) Modeling of loops in protein structures. *Protein Sci.*, **9**, 1753–1773.
29. Cheatham,T.E. III, Cieplak,P. and Kollman,P.A. (1999) A modified version of the Cornell *et al.* force field with improved sugar pucker phases and helical repeat. *J. Biomol. Struct. Dyn.*, **16**, 845–862.
30. Pearlman,D.A., Case,D.A., Caldwell,J.W., Ross,W.S., Cheatham,T.E., Debolt,S., Ferguson,D., Seibel,G. and Kollman,P. (1995) Amber, a package of computer-programs for applying molecular mechanics, normal-mode analysis, molecular-dynamics and free-energy calculations to simulate the structural and energetic properties of molecules. *Comput. Phys. Commun.*, **91**, 1–41.
31. Polkinghorne,A., Ziegler,U., Gonzalez-Hernandez,Y., Pospischil,A., Timms,P. and Vaughan,L. (2008) Chlamydophila pneumoniae HflX belongs to an uncharacterized family of conserved GTPases and associates with the *Escherichia coli* 50S large ribosomal subunit. *Microbiology*, **154**, 3537–3546.